

Theoretical predictions of melting behaviors of hcp iron up to 4000 GPa

Tran Dinh Cuong *

Faculty of Materials Science and Engineering, Phenikaa University, Hanoi 12116, Vietnam

Nguyen Quang Hoc , Nguyen Duc Trung, and Nguyen Thi Thao

Faculty of Physics, Hanoi National University of Education, Hanoi 11310, Vietnam

Anh D. Phan 

Faculty of Materials Science and Engineering, Phenikaa University, Hanoi 12116, Vietnam

and Phenikaa Institute for Advanced Study (PIAS), Phenikaa University, Hanoi 12116, Vietnam



(Received 8 May 2022; revised 24 August 2022; accepted 30 August 2022; published 16 September 2022)

The high-pressure melting diagram of iron is a vital ingredient for the geodynamic modeling of planetary interiors. Nonetheless, available data for molten iron show an alarming discrepancy. Herein, we propose an efficient one-phase approach to capture the solid-liquid transition of iron under extreme conditions. Our basic idea is to extend the statistical moment method to determine the density of iron in the TPa region. On that basis, we adapt the work-heat equivalence principle to appropriately link equation-of-state parameters with melting properties. This strategy allows explaining cutting-edge experimental and *ab initio* results without massive computational workloads. Our theoretical calculations would be helpful to constrain the chemical composition, internal dynamics, and thermal evolution of the Earth and super-Earths.

DOI: [10.1103/PhysRevB.106.094103](https://doi.org/10.1103/PhysRevB.106.094103)

I. INTRODUCTION

The melting process of compressed iron has acquired immense attention from the geophysical community. According to seismological and cosmochemical evidence, more than 80% of the Earth's core is constituted of this transition metal [1]. Hence, its melting information between 135 and 330 GPa is crucial for considering the Earth's thermal profile [2], heat flow [3], and magnetic field [4]. Furthermore, in recent years, 1569 super-Earths have been discovered outside our solar system [5]. Since these exoplanets can be tenfold heavier than the Earth, investigating their formation, evolution, and habitability requires a deep understanding of molten iron at extraordinary pressures up to 4000 GPa [6].

The past four decades witnessed arduous efforts to explore the melting characteristics of iron in deep-planetary interiors. On the experimental side, diamond anvil cell (DAC) [7–9] and shock-wave (SW) [10–14] techniques have been continuously improved. Unfortunately, the accurate melting curve of iron is clouded by numerous controversial results [15]. At 330 GPa, the reported melting temperatures exhibit a drastic scatter from 4850 to 7600 K. Therefore, determining the Earth's structure, dynamics, and history remains a major problem. Besides, it is challenging to access the TPa regime via current DAC and SW measurements [16–18]. On the simulation side, the density functional theory (DFT) and the diffusion Monte Carlo (DMC) method were developed to yield insights into the melting phenomenon [19–21]. These powerful *ab initio*

approaches can evaluate both ionic and electronic contributions without empirical adjustable parameters. Nevertheless, using DFT and DMC codes necessitates enormous computational resources [22]. In addition, *ab initio* phase relations near the Earth's inner core boundary (ICB) are still hotly debated [23–25].

Lately, the statistical moment method (SMM) has emerged as a promising quantum-mechanical tool for predicting the melting behaviors of metallic systems [26–28]. The SMM can describe the atomic rearrangement under various thermodynamic conditions via the quantum density matrix [29–31]. Based on the SMM equation of state (EOS), one often locates the melting point by analyzing the instability of the solid phase [26–28]. These approximations help enhance the computational efficiency dramatically [32]. A complete SMM run only takes ten seconds on a typical computer. However, SMM outputs for iron are inconsistent with each other [33–36]. Even at 135 GPa, the difference can be up to 30%. Moreover, existing SMM analyses [33–36] are limited to the ICB pressure of 330 GPa. Consequently, the melting mechanism of iron inside super-Earths remains a mystery to SMM researchers.

Herein, we formulate a simple but effective scheme to overcome SMM shortcomings. Theoretical calculations are primarily carried out for hcp iron because it is the leading candidate for planetary cores [37–40]. Our study is thoroughly compared with prior DAC, SW, *ab initio*, and SMM works.

II. EQUATION OF STATE

According to Cuong and Phan [35], the cohesive energy E_i of the i th iron atom can be well parameterized by the Morse

*cuong.trandinh@phenikaa-uni.edu.vn

model [41–43] as

$$E_i = \frac{1}{2} \sum_{j \neq i} D [e^{-2\alpha(r_{ij}-r_0)} - 2e^{-\alpha(r_{ij}-r_0)}], \quad (1)$$

where D is the potential depth, α^{-1} is the potential width, and r_0 is the critical value of the interatomic separation r_{ij} . This treatment is useful for accelerating computational processes and elucidating vibrational properties [35]. Thus, we keep utilizing the Morse function [41–43] to construct the SMM EOS for hcp iron. Specifically, $D = 0.6317$ eV, $\alpha = 1.4107 \text{ \AA}^{-1}$, and $r_0 = 2.6141 \text{ \AA}$ are extracted from recent DFT simulations [44]. On that basis, it is feasible to deduce quasi-harmonic and anharmonic force constants from the Leibfried-Ludwig theory [45] as

$$\begin{aligned} k_i &= \left(\frac{\partial^2 E_i}{\partial u_{i\delta}^2} \right)_{\text{eq}}, & \beta_i &= \left(\frac{\partial^3 E_i}{\partial u_{i\delta} \partial u_{i\eta}^2} \right)_{\text{eq}}, \\ \gamma_{1i} &= \left(\frac{\partial^4 E_i}{\partial u_{i\delta}^4} \right)_{\text{eq}}, & \gamma_{2i} &= \left(\frac{\partial^4 E_i}{\partial u_{i\delta}^2 \partial u_{i\eta}^2} \right)_{\text{eq}}, \end{aligned} \quad (2)$$

where $u_{i\delta}$ and $u_{i\eta}$ indicate atomic displacements along Cartesian axes ($\delta \neq \eta = x, y, z$). For simplicity, their average values are supposed to satisfy the following symmetric criterion:

$$\langle u_{i\delta} \rangle = \langle u_{i\eta} \rangle = \langle u_i \rangle. \quad (3)$$

In the thermodynamic equilibrium, if the i th atom is impacted by a supplemental force f_i , its movement will be governed by [46]

$$k_i \langle u_i \rangle + \beta_i \langle u_i^2 \rangle + (\frac{1}{6} \gamma_{1i} + \gamma_{2i}) \langle u_i^3 \rangle - f_i = 0. \quad (4)$$

Interestingly, the SMM enables us to associate the first-order moment ($\langle u_i \rangle$) with its high-order counterparts ($\langle u_i^2 \rangle$ and $\langle u_i^3 \rangle$) via [29–31]

$$\langle u_i^2 \rangle = \langle u_i \rangle^2 + \theta \frac{\partial \langle u_i \rangle}{\partial f_i} + \frac{\theta}{k_i} (x_i \coth x_i - 1), \quad (5)$$

$$\begin{aligned} \langle u_i^3 \rangle &= \langle u_i \rangle^3 + 3\theta \langle u_i \rangle \frac{\partial \langle u_i \rangle}{\partial f_i} \\ &\quad + \theta^2 \frac{\partial^2 \langle u_i \rangle}{\partial f_i^2} + \frac{\theta}{k_i} (x_i \coth x_i - 1) \langle u_i \rangle, \end{aligned} \quad (6)$$

where $\theta = k_B T$ is the Boltzmann constant k_B times the absolute temperature T , $x_i = \hbar \omega_i / 2\theta$ denotes the scaled phonon energy, \hbar stands for the reduced Planck constant, and ω_i represents the Einstein frequency. Inserting these statistical correlations into Eq. (4) gives us

$$\begin{aligned} \gamma_i \theta^2 \frac{d^2 y_i}{df_i^{*2}} + 3\gamma_i \theta y_i \frac{dy_i}{df_i^*} + \gamma_i y_i^3 + K_i y_i \\ + \frac{\gamma_i \theta}{k_i} (x_i \coth x_i - 1) y_i - f_i^* = 0, \end{aligned} \quad (7)$$

where

$$\begin{aligned} \gamma_i &= \frac{1}{6} \gamma_{1i} + \gamma_{2i}, & K_i &= k_i - \frac{\beta_i^2}{3\gamma_i}, & y_i &= \langle u_i \rangle + \frac{\beta_i}{3\gamma_i}, \\ f_i^* &= f_i - \frac{\beta_i k_i}{3\gamma_i} \left[\frac{2\beta_i^2}{9\gamma_i k_i} + \frac{2\gamma_i \theta}{k_i^2} (x_i \coth x_i - 1) - 1 \right]. \end{aligned} \quad (8)$$

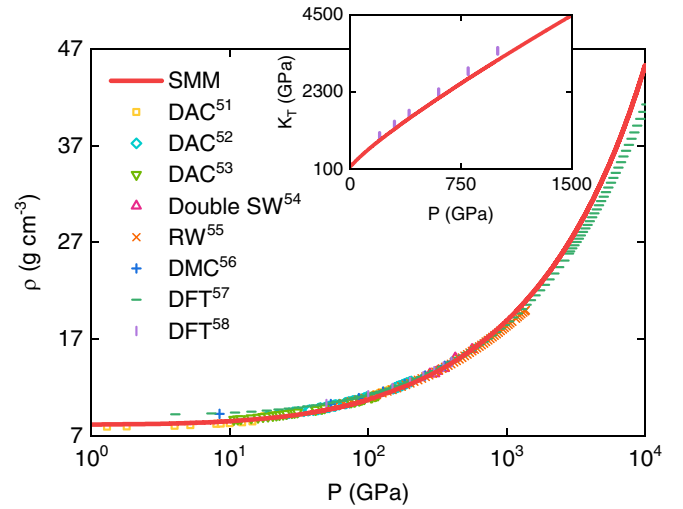


FIG. 1. The room-temperature SMM EOS of iron in comparison with recent measured and simulated results [51–58]. Inset: The pressure dependence of the isothermal bulk modulus given by SMM analyses and DFT calculations [58].

Notably, since f_i^* is arbitrarily small, we can express y_i as a polynomial function of f_i^* , which is

$$y_i = y_{i0} + A_{1i} f_i^* + A_{2i} f_i^{*2}, \quad (9)$$

where A_{1i} and A_{2i} are Taylor-Maclaurin coefficients. Applying the Tang-Hung iterative technique [47] to Eqs. (7) to (9) provides

$$\begin{aligned} y_{i0} &= \sqrt{\frac{2\gamma_i \theta^2}{3K_i^3} A_i}, \\ A_{1i} &= \frac{1}{K_i} \left[1 + \frac{2\gamma_i^2 \theta^2}{K_i^4} \left(1 + \frac{x_i \coth x_i}{2} \right) (1 + x_i \coth x_i) \right], \\ A_{2i} &= \frac{1}{2K_i y_{i0}} \left[\frac{1}{3K_i} (1 - x_i \coth x_i) - \frac{1}{K_i} - \frac{y_{i0}^2}{\theta} \right]. \end{aligned} \quad (10)$$

The explicit form of A_i was extensively reported in previous SMM literature [48–50]. Consequently, when f_i goes to zero, $\langle u_i \rangle$ is estimated by

$$\begin{aligned} \langle u_i \rangle &\approx \sqrt{\frac{2\gamma_i \theta^2}{3K_i^3} A_i} - \frac{\beta_i}{3\gamma_i} \\ &\quad + A_{1i} \frac{\beta_i k_i}{3\gamma_i} \left[1 - \frac{2\beta_i^2}{9\gamma_i k_i} - \frac{2\gamma_i \theta}{k_i^2} (x_i \coth x_i - 1) \right]. \end{aligned} \quad (11)$$

In other words, we can obtain the density ρ of hcp iron from [35]

$$\rho(P, T) = \frac{m_i \sqrt{2}}{[a_i(P, 0) + \langle u_i \rangle(P, T)]^3}, \quad (12)$$

where P is the hydrostatic pressure, m_i is the atomic mass, and a_i is the mean nearest-neighbor distance.

Numerical calculations relying on Eq. (12) are shown in Fig. 1. It is conspicuous that hcp iron becomes significantly denser during isothermal squeezing. At room temperature, a sharp growth of 37.17 g cm^{-3} is recorded in ρ between 0 and

10 000 GPa. Our SMM analyses agree quantitatively with static DAC measurements [51–53], multishock experiments [54], ramp-wave (RW) investigations [55], and DFT/DMC computations [56–58]. The deviation between the SMM and other state-of-the-art methods [51–58] is less than 10% over a vast pressure range. A better consensus can be reached by adding magnetic terms [51,59] to *ab initio* EOSs [56–58] at $P \leq 50$ GPa. Hence, our SMM results would be valuable for constraining the chemical composition of extrasolar bodies up to ten Earth masses (see Appendix A). To facilitate geodynamic modeling, we fit SMM data by the Vinet EOS [60] as

$$P = 3K_0\xi^{-2}(1 - \xi)\exp\left[\frac{3}{2}(K'_0 - 1)(1 - \xi)\right], \quad (13)$$

where $\xi = (\rho_0/\rho)^{1/3}$, $\rho_0 = 8.13 \text{ g cm}^{-3}$, $K_0 = 175.34$ GPa, and $K'_0 = 5.02$. Equation (13) allows us to consider compression effects on the bulk modulus K_T by

$$K_T = K_0 \left[\frac{3(1 - K'_0)}{2} + \frac{3K'_0 - 5}{2\xi} + \frac{2}{\xi^2} \right] \times \exp\left[\frac{3}{2}(K'_0 - 1)(1 - \xi)\right]. \quad (14)$$

Excitingly, even for K_T , the SMM output only differs from the latest DFT one [58] by 7.58% at 1000 GPa. This consistency reaffirms the reliability of the SMM EOS.

III. MELTING BEHAVIORS

It cannot be denied that there is a tight connection between the EOS and other physical properties. In particular, numerous attempts were made to derive melting quantities from EOS parameters [61–63]. Lately, Ma *et al.* [64] introduced a semi-empirical approach, called the work-heat equivalence principle (WHEP), to handle this long-standing issue. In the WHEP picture [64], a liquid can be crystallized owing to exothermic or distortion influences. Therefore, heat energies during isobaric cooling are analogous to mechanical works during isothermal squeezing. This unique point of view [64] helps determine the melting temperature T^m by

$$T^m(P) = T_1(P_1) + [T_2(P_2) - T_1(P_1)] \sqrt{\frac{\int_{\xi_1}^{\xi} P(\xi')\xi'^2 d\xi'}{\int_{\xi_1}^{\xi_2} P(\xi')\xi'^2 d\xi'}}, \quad (15)$$

where (T_1, P_1, ξ_1) and (T_2, P_2, ξ_2) are two reference melting points. Based on the Murnaghan approximation [65], Ma *et al.* [64] explicitly rewrote Eq. (15) by

$$T^m(P) = T_1(P_1) + [T_2(P_2) - T_1(P_1)] \times \frac{\left(\frac{K'_0 P + K_0}{K'_0 P_1 + K_0}\right)^{-\frac{1}{K'_0}} \left(\frac{P + K_0}{P_1 + K_0}\right) - 1}{\left(\frac{K'_0 P_2 + K_0}{K'_0 P_1 + K_0}\right)^{-\frac{1}{K'_0}} \left(\frac{P_2 + K_0}{P_1 + K_0}\right) - 1}. \quad (16)$$

Equation (16) has been successfully applied to various metallic substances [64] and ionic compounds [66]. Notwithstanding, all WHEP predictions [64,66] have been restricted to $P \sim 2K_0$. A viable solution for the WHEP problem is to replace the Murnaghan EOS with the SMM EOS [63]. Com-

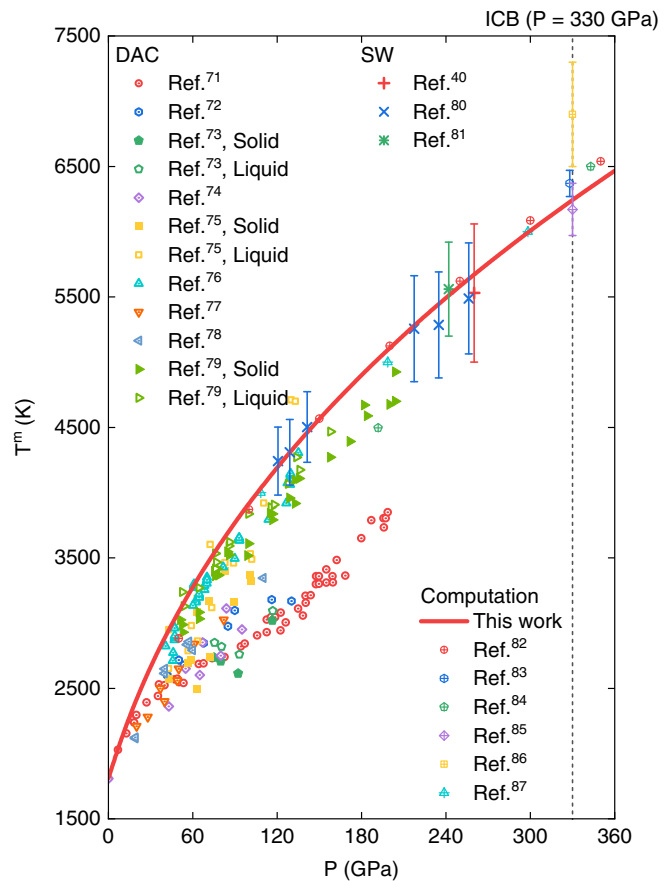


FIG. 2. The melting profile of iron inferred from our SMM-WHEP analyses, DAC experiments [71–79], SW measurements [40,80,81], *ab initio* calculations [82–86], and atomistic simulations adopting machine-learning potentials [87] in a pressure range from 0 to 360 GPa.

bining Eqs. (13) and (15) yields

$$T^m(P) = T_1(P_1) + [T_2(P_2) - T_1(P_1)] \sqrt{\frac{W(\xi) - W(\xi_1)}{W(\xi_2) - W(\xi_1)}},$$

$$W(\xi) = \left[1 + \frac{3}{2}(K'_0 - 1)(\xi - 1)\right] \exp\left[\frac{3}{2}(K'_0 - 1)(1 - \xi)\right]. \quad (17)$$

The effectiveness of Eq. (17) is thoroughly demonstrated in the Supplemental Material [67]. In this section, Eq. (17) is employed to decode the melting behaviors of iron at deep-planetary conditions. For objectivity, we choose $P_1 = 0$ GPa, $T_1 = 1811$ K, $P_2 = 5.2$ GPa, and $T_2 = 1991$ K [68]. This low-pressure melting information has been widely validated by different research groups [69,70].

Figure 2 shows the melting properties of iron inside the Earth. In general, there are three principal scenarios for its melting process under extreme compression. First, Boehler *et al.* [71,72], Aquilanti *et al.* [73], and Basu *et al.* [74] recommended a relatively flat melting curve for iron. They predicted a slight increase in T^m to 4850 ± 200 K at 330 GPa [71–74]. However, their DAC data [71–74] may have been misinterpreted due to the contamination [75] or deformation

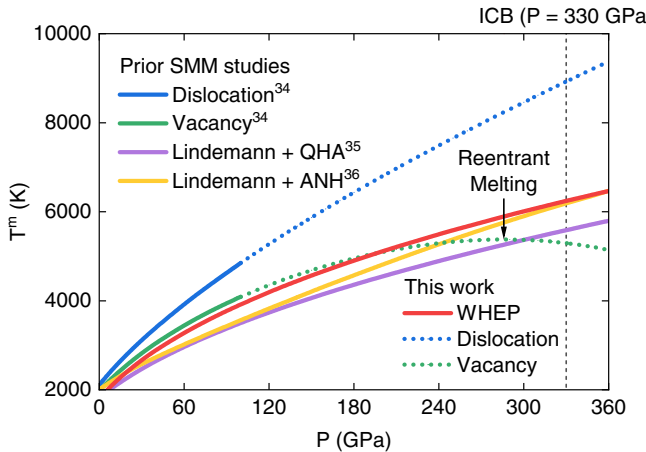


FIG. 3. Influences of hydrostatic compression on the melting point of iron derived from our current research and previous SMM investigations [34–36]. QHA and ANH stand for quasi-harmonic and anharmonic approximations, respectively.

[76] of iron samples. Second, Jackson *et al.* [77] and Zhang *et al.* [78] suggested that iron should melt in the intermediate-temperature region. Extrapolating their DAC results [77,78] to 330 GPa has provided $T^m = 5700 \pm 200$ K. Unfortunately, this value may have been underestimated because of the inaccurate treatment of thermal pressures [75]. Finally, a steep melting line for iron was explored by Anzellini *et al.* [79], Morard *et al.* [75], and Hou *et al.* [76]. Their DAC studies [75,76,79] found $T^m = 6230 \pm 500$ K at the ICB. This melting characteristic of iron was reconfirmed by cutting-edge SW measurements of Li *et al.* [80] ($T^m = 5950 \pm 400$), Turneaure *et al.* [81] ($T^m \sim 6400$ K), and Kraus *et al.* [40] ($T^m = 6230 \pm 540$ K).

Our SMM-WHEP calculations strongly support the last experimental scenario [40,75,76,79–81]. Specifically, the SMM-WHEP melting temperature climbs sharply from 4384 K at 135 GPa to 6243 K at 330 GPa. This melting tendency is in line with our two-phase simulations in the Supplemental Material [67]. Furthermore, excellent accordance among SMM-WHEP, DFT [82–85], DMC [86], and machine-learning [87] outputs is achieved. Thus, the true melting profile of iron may be extremely close to our solid-liquid boundary. Our SMM-WHEP findings would have profound geophysical implications for the Earth's dynamics and evolution (see Appendix B).

Remarkably, this is the first time the SMM and other approaches [40,75,76,79–87] have been consolidated in a unified picture. For clarity, we compare available SMM melting diagrams in Fig. 3. Pioneering SMM works [33,34] utilized the dislocation-mediated melting theory [63,88,89] to investigate the melting event of iron as

$$\frac{\mu}{\rho T^m} = \text{const.}, \quad (18)$$

where μ is the shear modulus. Although Eq. (18) can be straightforwardly solved, the obtained melting point is often overestimated [90–92]. For example, at the ICB, Eq. (18) gives us $T^m = 8923$ K, which is far beyond *ab initio* outputs [82–86]. To address the mentioned drawback, Hoc *et al.* [34]

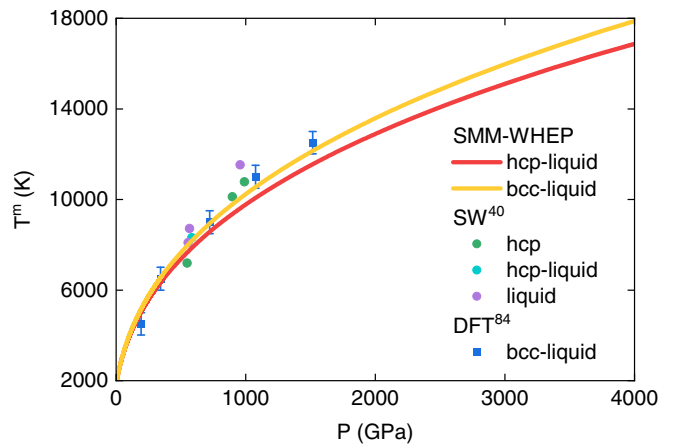


FIG. 4. The melting temperature of iron as a function of super-Earth pressure gained from our SMM-WHEP calculations, laser-driven SW experiments [40], and DFT two-phase simulations [84].

took into account the impact of point defects by

$$\Delta T^m = \left(\frac{\partial T}{\partial c_V} \right)_{\rho, P} c_V = \frac{2k_B T^m}{T^m \frac{\partial E_i}{\partial T} - E_i}, \quad (19)$$

where ΔT^m is the temperature correction and c_V is the mono-vacancy concentration. The SMM analyses of Hoc *et al.* [34] are compatible with the DFT free-energy computations of Alfe *et al.* [82] at $P \leq 100$ GPa. Nonetheless, when extending their idea to denser systems, we observe the presence of reentrant melting at 286 GPa and 5376 K. This strange phenomenon is most likely a consequence of ignoring the vacancy formation volume [28].

Apart from defective models [33,34], the melting transition of iron has been related to its vibrational instability via the Lindemann criterion [93–95] as

$$\frac{\langle u_i^2 \rangle}{a_i^2} = \text{const.} \quad (20)$$

Cuong and Phan [35] accurately reproduced high-quality DAC data of Morard *et al.* [75] by solving Eq. (20) within the quasi-harmonic approximation. Nevertheless, a slight underestimation of the melting temperature was recorded at $P \geq 135$ GPa [35]. Tan and Tam [36] revealed that the situation can be improved by performing fully anharmonic SMM calculations. As presented in Fig. 3, their numerical results [36] are quantitatively consistent with our SMM-WHEP predictions. However, from our perspective, the above agreement is just an accident. Indeed, Tan and Tam [36] used the Lennard-Jones pairwise potential [96] to formulate the SMM EOS. This method often causes an overestimation of the scaled atomic volume [97–99]. At 330 GPa, ξ^3 for the Lennard-Jones iron was reported to be 0.72 [36], about 22% larger than the DAC value [51–53].

Figure 4 illustrates the melting curve of iron under super-Earth conditions. Overall, SMM-WHEP outputs are somewhat lower than their DFT counterparts [84]. At 1517 GPa, our present SMM-WHEP analyses provide $T^m = 11560$ K, whereas earlier DFT simulations of Bouchet *et al.* [84]

TABLE I. Simon-Glatzel parameters for hcp iron and bcc iron.

Phase	T^*	P^*	b	c
hcp	1811 K	0 GPa	16.88 GPa	2.44
bcc	1811 K	0 GPa	16.86 GPa	2.38

yielded $T^m = 12\,506$ K. This discrepancy primarily originated from the selection of initial crystalline structures. Unlike us, Bouchet *et al.* [84] focused on bcc iron. According to Belonoshko *et al.* [25], the bcc-liquid boundary can be slightly higher than the hcp-liquid one. To be more specific, we reapply the SMM-WHEP scheme to the bcc phase with $0 \leq P \leq 4000$ GPa. Fascinatingly, while K'_0 is almost unchanged, K_0 rises by a factor of 1.13. These findings are bolstered by modern thermodynamic calculations of Dorogokupets *et al.* [70]. Hence, our high-pressure melting line becomes steeper and passes through all DFT points [84] within the error bars.

Despite the achieved agreement, it should be emphasized that the real phase diagram of iron remains mysterious. Experimentalists only detected the melting signatures of hcp iron at above 100 GPa [40]. On the other hand, large-scale *ab initio* computations indicated that bcc iron can be dynamically stabilized due to superionic-like diffusion at elevated temperatures [23]. More efforts are essential to answer what phase of iron exists in planetary cores.

For convenience, we parametrize SMM-WHEP melting profiles by the semi-empirical Simon-Glatzel law [100], which is

$$T^m = T^* \left(\frac{P - P^*}{b} + 1 \right)^{\frac{1}{c}}. \quad (21)$$

Our fitted results for T^* , P^* , b , and c are listed in Table I. They can be utilized to consider the thermophysical state of rocky exoplanets (see Appendix C).

IV. CONCLUSION

The SMM-WHEP has been successfully developed to shed light on the melting behaviors of iron under intense compression up to 4000 GPa. This one-phase approach enables us to directly infer high-pressure melting properties from equation-of-state parameters. On that basis, we quantitatively explained previous DAC/SW experiments, DFT/DMC simulations, and SMM calculations with minimal computational cost. Therefore, our theoretical information about molten iron would be valuable for advancing knowledge of planetary interiors. It is practicable to extend our SMM-WHEP analyses to more complex minerals.

ACKNOWLEDGMENTS

We thank two anonymous referees for their valuable comments and suggestions.

APPENDIX A: MASS-RADIUS RELATIONSHIP

Mass (M) and radius (R) are the only observable characteristics for most super-Earths. To predict their chemical structures, one needs to compare the measured results for M

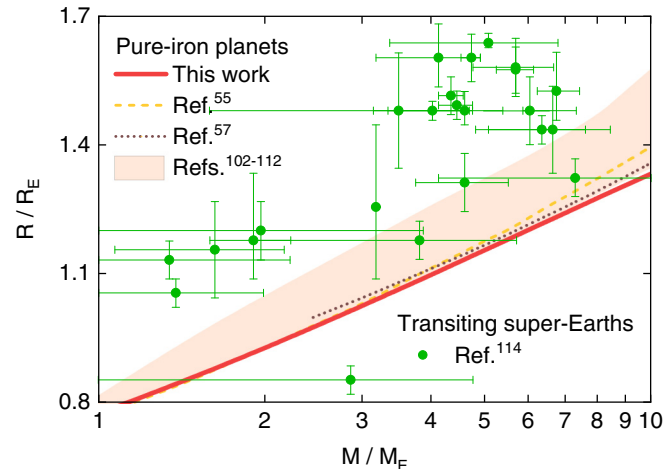


FIG. 5. The mass-radius correlation of hypothetical pure-iron planets provided by our SMM study and Refs. [55,57,102–112]. Experimental data for transiting super-Earths [114] are also plotted for comparison.

and R with the calculated M - R curves of candidate materials [101]. Notwithstanding, theoretical M - R diagrams often show wide variations owing to the lack of EOS data at the TPa regime [102–112]. In this Appendix, we adopt the SMM EOS to determine the M - R relationship of homogeneous iron planets. Fundamentally, their hydrostatic equilibrium can be well described by [108]

$$\frac{dP(r)}{dr} = -g(r)\rho(r), \quad (A1)$$

where g is the Newtonian gravitational acceleration. Employing the Gauss theorem gives us [108]

$$\frac{dg(r)}{dr} = 4\pi G\rho(r) - 2\frac{g(r)}{r}, \quad (A2)$$

where G is the Newtonian constant of gravitation. For a given value of the core pressure P_c , we numerically solve Eqs. (13), (A1), and (A2) from the planetary center ($r \rightarrow 0$, $P \rightarrow P_c$, $g \rightarrow 0$) to the planetary surface ($r \rightarrow R$, $P \rightarrow 0$, $g \rightarrow g_s$). After obtaining R and g_s , we can readily compute M by [108]

$$M = \frac{g_s}{G}R^2. \quad (A3)$$

Figure 5 illustrates how R/R_E depends on M/M_E in the case of pure-iron celestial bodies. Here, R_E and M_E are the Earth's radius and mass, respectively. It is clear to see that R/R_E grows monotonically with M/M_E . For instance, R/R_E increases from 0.77 to 1.33 when M/M_E climbs from 1 to 10. Our SMM analyses are in consonance with the *ab initio* simulations of Hakim *et al.* [57]. The maximum difference between these approaches is merely 2.30%.

Notably, some prior studies [113] suggested the existence of superdense exoplanets. These anomalous objects are markedly heavier than homogeneous iron spheres of the same size. However, according to our theoretical calculations, the probability of detecting them is extremely low. Most of the observed M - R points [114] locate above our M - R boundary, except for a few rare circumstances with large uncertainties.

TABLE II. Thermophysical parameters needed for the Buffett model [115]. dT^m/dP , dT^s/dP , L , γ_G , K_S , C_P , and $\Delta\rho_{\text{ICB}}$ are considered at the ICB, whereas Q is defined at the Earth's core-mantle boundary.

Symbol	Physical meaning	Specific value	Reference
dT^m/dP	Clapeyron slope	7.7 K GPa^{-1}	This work
dT^s/dP	Adiabatic gradient	5.8 K GPa^{-1}	Ref. [4]
L	Fusion enthalpy	10^6 J kg^{-1}	Ref. [85]
γ_G	Gruneisen parameter	1.39	Ref. [116]
K_S	Adiabatic bulk modulus	1306 GPa	Ref. [116]
C_P	Isobaric heat capacity	$790 \text{ J kg}^{-1} \text{ K}^{-1}$	Ref. [116]
r_{IC}	Inner-core radius	1221 km	Ref. [117]
r_{OC}	Outer-core radius	3480 km	Ref. [117]
ρ_{avg}	Outer-core mean density	$12\,000 \text{ kg m}^{-3}$	Ref. [117]
$\Delta\rho_{\text{ICB}}$	Compositional density jump	620 kg m^{-3}	Ref. [118]
Q	Heat flow	10 TW	Ref. [119]

Our conclusion is forcefully supported by the state-of-the-art RW experiments of Smith *et al.* [55].

APPENDIX B: AGE OF THE EARTH'S INNER CORE

The Earth's core has been solidified from the bottom up. To estimate the interval τ between the crystallization onset and the present time, we use the energy-conservation model of Buffett, which is [115]

$$\tau = \frac{\mathcal{M}}{Q} \left[\left(\frac{r_{\text{IC}}}{r_{\text{OC}}} \right)^2 + \mathcal{L} \left(\frac{r_{\text{IC}}}{r_{\text{OC}}} \right)^3 + \mathcal{G} \left(\frac{r_{\text{IC}}}{r_{\text{OC}}} \right)^3 \right], \quad (\text{B1})$$

where

$$\begin{aligned} \mathcal{M} &= 4\pi \left(\frac{1}{3} - \frac{1}{5} \frac{Ar_{\text{OC}}^2 \gamma_G}{K_S} \right) \rho_{\text{avg}} C_P Ar_{\text{OC}}^5 \left(\frac{dT^m}{dP} - \frac{dT^s}{dP} \right), \\ A &= \frac{2\pi}{3} G \rho_{\text{avg}}^2, \quad \mathcal{L} = \frac{A\pi}{3} \frac{\rho_{\text{avg}} L r_{\text{OC}}^3}{\mathcal{M}}, \\ \mathcal{G} &= \frac{4\pi}{5} \frac{Ar_{\text{OC}}^5}{\mathcal{M}} \frac{\Delta\rho_{\text{ICB}}}{\rho_{\text{avg}}}. \end{aligned} \quad (\text{B2})$$

Details about these thermophysical parameters are presented in Table II [4,85,116–119]. On that basis, we get $\tau = 0.44$ Gyr. This figure implies that our planet has a young solid inner core [80]. Our physical picture is very consistent with recent DFT and paleomagnetic explorations [120,121] ($\tau = 0.4 – 0.7$ Gyr).

APPENDIX C: STATE OF TERRESTRIAL EXOPLANETS

It is well known that the habitability of super-Earths depends crucially on the thermodynamic state of their cores [122]. Unfortunately, too many contradictory scenarios have been proposed. For example, Valencia *et al.* [123] predicted that super-Earth cores would be completely solid. In contrast, Sotin *et al.* [124] argued that these systems would be entirely liquid. Additionally, some other scientists suggested that the core solidification would occur from the top down via iron snowflake-like mechanisms [125]. These persisting controversies principally stem from the scarcity of ultrahigh-pressure melting information.

Here, we apply SMM-WHEP results to deal with the mentioned issues. First of all, we evaluate the depression effect of

light elements (e.g., S, O, and Si) on the melting transition of hcp iron via the cryoscopic equation as [126]

$$T_{\text{alloy}}^m = \frac{T^m}{1 - \ln(1 - x^*)} = \frac{T^*}{1 - \ln(1 - x^*)} \left(\frac{P - P^*}{b} + 1 \right)^{\frac{1}{c}}, \quad (\text{C1})$$

where $x^* = 0.13$ is the mole fraction of impurities. Next, the temperature distribution in deep-planetary interiors is determined by the adiabatic method as [126]

$$\frac{\partial \ln T_{\text{core}}}{\partial \ln \rho_{\text{core}}} = \gamma_G. \quad (\text{C2})$$

The core density ρ_{core} and the Gruneisen parameter γ_G are taken from high-quality *ab initio* datasets of STIXRUEDE [127]. Meanwhile, the initial value of T_{core} at the core-mantle interface is deduced from the latest SW measurements of Fei *et al.* [128]. Finally, the fundamental physical structure of super-Earth cores is elucidated by comparing T_{alloy}^m with T_{core} .

Figure 6 shows our representative numerical calculations for a ten-Earth-mass celestial body with a partially molten silicate mantle. It is conspicuous that T_{alloy}^m is lower than T_{core} at the uppermost core ($P \sim 1350$ GPa [18]). Nevertheless, the melting slope is appreciably higher than the adiabatic gradient. These events lead to the intersection of the melting curve

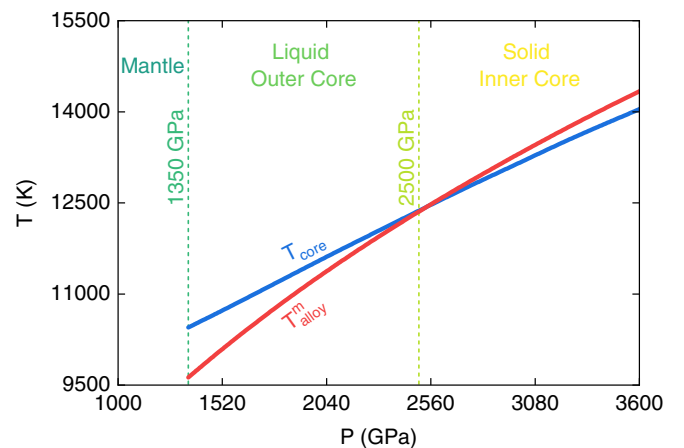


FIG. 6. Our theoretical predictions for the core crystallization of a telluric exoplanet with $M = 10M_E$.

and the adiabatic line at around 2500 GPa. In other words, similar to our planet, the studied super-Earth has both a molten outer core and a frozen inner core. Thus, the generation of its magnetic field can be efficiently promoted by the churning of

liquid iron-based alloys [129,130]. This magnetic shield helps protect organic life forms from dangerous cosmic radiation [129,130]. Our findings concur with the leading-edge SW experiments of Kraus *et al.* [40].

-
- [1] K. Hirose, B. Wood, and L. Vocablo, *Nat. Rev. Earth Environ.* **2**, 645 (2021).
- [2] R. Sinmyo, K. Hirose, and Y. Ohishi, *Earth Planet. Sci. Lett.* **510**, 45 (2019).
- [3] Y. Zhang, T. Sekine, J. F. Lin, H. He, F. Liu, M. Zhang, T. Sato, W. Zhu, and Y. Yu, *J. Geophys. Res. Solid Earth* **123**, 1314 (2018).
- [4] C. Davies, M. Pozzo, D. Gubbins, and D. Alfe, *Nat. Geoscience* **8**, 678 (2015).
- [5] Latest data from NASA's Exoplanet Archive: <https://exoplanets.nasa.gov/discovery/>, (accessed May 2022).
- [6] T. Duffy, N. Madhusudhan, and K. K. M. Lee, *Treatise on Geophysics*, 2nd ed., (Elsevier, Amsterdam, 2015), Vol. 2, p. 149.
- [7] Q. Williams, R. Jeanloz, J. Bass, B. Svendsen, and T. J. Ahrens, *Science* **236**, 181 (1987).
- [8] G. Shen, V. B. Prakapenka, M. L. Rivers, and S. R. Sutton, *Phys. Rev. Lett.* **92**, 185701 (2004).
- [9] Y. Fei, *Science* **340**, 442 (2013).
- [10] J. M. Brown and R. G. McQueen, *J. Geophys. Res.* **91**, 7485 (1986).
- [11] J. D. Bass, B. Svendsen, and T. J. Ahrens, in *High Pressure Research in Mineral Physics*, edited by M. H. Manghanani and Y. Syono (American Geophysical Union, Washington, DC, 1987), p. 393.
- [12] C. S. Yoo, N. C. Holmes, M. Ross, D. J. Webb, and C. Pike, *Phys. Rev. Lett.* **70**, 3931 (1993).
- [13] J. H. Nguyen and N. C. Holmes, *Nature (London)* **427**, 339 (2004).
- [14] H. Tan, C. D. Dai, L. Y. Zhang, and C. H. Xu, *Appl. Phys. Lett.* **87**, 221905 (2005).
- [15] R. Boehler and M. Ross, *Treatise on Geophysics*, 2nd ed., (Elsevier, Amsterdam, 2015), Vol. 2, p. 573.
- [16] S. Anzellini and S. Boccato, *Crystals* **10**, 459 (2020).
- [17] P. Parisiades, *Crystals* **11**, 416 (2021).
- [18] T. S. Duffy and R. F. Smith, *Front. Earth Sci.* **7**, 23 (2019).
- [19] D. Alfe, *Rev. Mineral. Geochem.* **71**, 337 (2010).
- [20] D. Alfe, *Treatise on Geophysics*, 2nd ed., (Elsevier, Amsterdam, 2015), Vol. 2, p. 369.
- [21] S. Mazevert, R. Musella, and F. Guyot, *Astron. Astrophys.* **631**, L4 (2019).
- [22] L. F. Zhu, B. Grabowski, and J. Neugebauer, *Phys. Rev. B* **96**, 224202 (2017).
- [23] A. B. Belonoshko, T. Lukinov, J. Fu, J. Zhao, S. Davis, and S. I. Simak, *Nat. Geoscience* **10**, 312 (2017).
- [24] A. J. Schultz, S. G. Moustafa, and D. A. Kofke, *Sci. Rep.* **8**, 7295 (2018).
- [25] A. B. Belonoshko, J. Fu, and G. Smirnov, *Phys. Rev. B* **104**, 104103 (2021).
- [26] H. K. Hieu, *J. Appl. Phys.* **116**, 163505 (2014).
- [27] T. D. Cuong, N. Q. Hoc, and A. D. Phan, *J. Appl. Phys.* **125**, 215112 (2019).
- [28] T. D. Cuong and A. D. Phan, *Vacuum* **179**, 109444 (2020).
- [29] K. Masuda-Jindo, V. V. Hung, and P. D. Tam, *Phys. Rev. B* **67**, 094301 (2003).
- [30] K. Masuda-Jindo, S. R. Nishitani, and V. VanHung, *Phys. Rev. B* **70**, 184122 (2004).
- [31] N. Van Nghia, H. K. Hieu, and D. D. Phuong, *Vacuum* **196**, 110725 (2022).
- [32] T. D. Cuong and A. D. Phan, *Phys. Chem. Chem. Phys.* **24**, 4910 (2022).
- [33] L. T. C. Tuyen, N. Q. Hoc, B. D. Tinh, D. Q. Vinh, and T. D. Cuong, *Chin. J. Phys.* **59**, 1 (2019).
- [34] N. Q. Hoc, L. H. Viet, and N. T. Dung, *J. Electron. Mater.* **49**, 910 (2020).
- [35] T. D. Cuong and A. D. Phan, *Vacuum* **185**, 110001 (2021).
- [36] P. D. Tan and P. D. Tam, *Eur. Phys. J. B* **95**, 7 (2022).
- [37] Y. Kuwayama, K. Hirose, N. Sata, and Y. Ohishi, *Earth Planet. Sci. Lett.* **273**, 379 (2008).
- [38] S. Tateno, K. Hirose, Y. Ohishi, and Y. Tatsumi, *Science* **330**, 359 (2010).
- [39] B. K. Godwal, F. Gonzalez-Cataldo, A. K. Verma, L. Stixrude, and R. Jeanloz, *Earth Planet. Sci. Lett.* **409**, 299 (2015).
- [40] R. G. Kraus, R. J. Hemley, S. J. Ali, J. L. Belof, L. X. Benedict, J. Bernier, D. Braun, R. E. Cohen, G. W. Collins, F. Coppari, M. P. Desjarlais, D. Fratanduono, S. Hamel, A. Krygier, A. Lazicki, J. McNamey, M. Millot, P. C. Myint, M. G. Newman, J. R. Rygg *et al.*, *Science* **375**, 202 (2022).
- [41] P. M. Morse, *Phys. Rev.* **34**, 57 (1929).
- [42] L. A. Girifalco and V. G. Weizer, *Phys. Rev.* **114**, 687 (1959).
- [43] I. V. Pirog and T. I. Nedoseikina, *Phys. B: Condens. Matter* **334**, 123 (2003).
- [44] Q. Ye, Y. Hu, X. Duan, H. Liu, H. Zhang, C. Zhang, L. Sun, W. Yang, W. Xu, Q. Cai, Z. Wang, and S. Jiang, *J. Synchrotron Radiat.* **27**, 436 (2020).
- [45] G. Leibfried and W. Ludwig, *Solid State Phys.* **12**, 275 (1961).
- [46] V. V. Hung, K. Masuda-Jindo, and P. T. M. Hanh, *J. Phys.: Condens. Matter* **18**, 283 (2006).
- [47] N. Tang and V. V. Hung, *Phys. Status Solidi B* **149**, 511 (1988).
- [48] V. Van Hung and N. T. Hai, *Comput. Mater. Sci.* **14**, 261 (1999).
- [49] D. D. Phuong, N. T. Hoa, V. V. Hung, D. Q. Khoa, and H. K. Hieu, *Eur. Phys. J. B* **89**, 84 (2016).
- [50] K. H. Ho, V. T. Nguyen, N. V. Nghia, N. B. Duc, V. Q. Tho, T. T. Hai, and D. Q. Khoa, *Curr. Appl. Phys.* **19**, 55 (2019).
- [51] A. Dewaele, P. Loubeyre, F. Occelli, M. Mezouar, P. I. Dorogokupets, and M. Torrent, *Phys. Rev. Lett.* **97**, 215504 (2006).
- [52] Y. Fei, C. Murphy, Y. Shibasaki, A. Shahar, and H. Huang, *Geophys. Res. Lett.* **43**, 6837 (2016).
- [53] F. Miozzi, J. Matas, N. Guignot, J. Badro, J. Siebert, and G. Fiquet, *Minerals* **10**, 100 (2020).
- [54] Y. Ping, F. Coppari, D. G. Hicks, B. Yaakobi, D. E. Fratanduono, S. Hamel, J. H. Eggert, J. R. Rygg, R. F. Smith, D. C. Swift, D. G. Braun, T. R. Boehly, and G. W. Collins, *Phys. Rev. Lett.* **111**, 065501 (2013).

- [55] R. F. Smith, D. E. Fratanduono, D. G. Braun, T. S. Duffy, J. K. Wicks, P. M. Celliers, S. J. Ali, A. Fernandez-Panella, R. G. Kraus, D. C. Swift, G. W. Collins, and J. H. Eggert, *Nat. Astron.* **2**, 452 (2018).
- [56] E. Sola, J. P. Brodholt, and D. Alfe, *Phys. Rev. B* **79**, 024107 (2009).
- [57] K. Hakim, A. Rivoldini, T. V. Hoolst, S. Cottenier, J. Jaeken, T. Chust, and G. Steinle-Neumann, *Icarus* **313**, 61 (2018).
- [58] J. Zhuang, H. Wang, Q. Zhang, and R. M. Wentzcovitch, *Phys. Rev. B* **103**, 144102 (2021).
- [59] G. Steinle-Neumann, R. E. Cohen, and L. Stixrude, *J. Phys.: Condens. Matter* **16**, S1109 (2004).
- [60] P. Vinet, J. Ferrante, J. H. Rose, and J. R. Smith, *J. Geophys. Res.* **92**, 9319 (1987).
- [61] N. Tang and V. V. Hung, *Phys. Status Solidi B* **162**, 379 (1990).
- [62] Y. Wang, R. Ahuja, and B. Johansson, *Phys. Rev. B* **65**, 014104 (2001).
- [63] L. Burakovsky, D. L. Preston, and R. R. Silbar, *J. Appl. Phys.* **88**, 6294 (2000).
- [64] J. Ma, W. Li, G. Yang, S. Zheng, Y. He, X. Zhang, X. Zhang, and X. Zhang, *Phys. Earth Planet. Inter.* **309**, 106602 (2020).
- [65] F. D. Murnaghan, *Proc. Natl. Acad. Sci. USA* **30**, 244 (1944).
- [66] T. D. Cuong and A. D. Phan, *Vacuum* **189**, 110231 (2021).
- [67] See Supplemental Material at <http://link.aps.org/supplemental/10.1103/PhysRevB.106.094103> to be inserted by publisher for our SMM-WHEP tests on some typical metals whose melting profiles were unambiguously measured and simulated at elevated pressures. Besides, in this document, classical molecular dynamics simulations are carried out to reinforce our SMM-WHEP predictions for molten iron. Supplemental Material includes Refs. [42,44,60,131–157].
- [68] L. J. Swartzendruber, *Bull. Alloy Phase Diagrams* **3**, 161 (1982).
- [69] L. Deng, C. Seagle, Y. Fei, and A. Shahar, *Geophys. Res. Lett.* **40**, 33 (2013).
- [70] P. I. Dorogokupets, A. M. Dymshtis, K. D. Litasov, and T. S. Sokolova, *Sci. Rep.* **7**, 41863 (2017).
- [71] R. Boehler, *Nature (London)* **363**, 534 (1993).
- [72] R. Boehler, D. Santamaria-Perez, D. Errandonea, and M. Mezouar, *J. Phys.: Conf. Ser.* **121**, 022018 (2008).
- [73] G. Aquilanti, A. Trapananti, A. Karandikar, I. Kantor, C. Marini, O. Mathon, S. Pasquarelli, and R. Boehler, *Proc. Natl. Acad. Sci. USA* **112**, 12042 (2015).
- [74] A. Basu, M. R. Field, D. G. McCulloch, and R. Boehler, *Geosci. Front.* **11**, 565 (2020).
- [75] G. Morard, S. Boccato, A. D. Rosa, S. Anzellini, F. Miozzi, L. Henry, G. Garbarino, M. Mezouar, M. Harmand, F. Guyot, E. Boulard, I. Kantor, T. Irifune, and R. Torchio, *Geophys. Res. Lett.* **45**, 11074 (2018).
- [76] M. Hou, J. Liu, Y. Zhang, X. Du, H. Dong, L. Yan, J. Wang, L. Wang, and B. Chen, *Geophys. Res. Lett.* **48**, e2021GL095739 (2021).
- [77] J. M. Jackson, W. Sturhahn, M. Lerche, J. Zhao, T. S. Toellner, E. E. Alp, S. V. Sinogeikin, J. D. Bass, C. A. Murphy, and J. K. Wicks, *Earth Planet. Sci. Lett.* **362**, 143 (2013).
- [78] D. Zhang, J. M. Jackson, J. Zhao, W. Sturhahn, E. E. Alp, M. Y. Hu, T. S. Toellner, C. A. Murphy, and V. B. Prakapenka, *Earth Planet. Sci. Lett.* **447**, 72 (2016).
- [79] S. Anzellini, A. Dewaele, M. Mezouar, P. Loubeyre, and G. Morard, *Science* **340**, 464 (2013).
- [80] J. Li, Q. Wu, J. Li, T. Xue, Y. Tan, X. Zhou, Y. Zhang, Z. Xiong, Z. Gao, and T. Sekine, *Geophys. Res. Lett.* **47**, e2020GL087758 (2020).
- [81] S. J. Turneaure, S. M. Sharma, and Y. M. Gupta, *Phys. Rev. Lett.* **125**, 215702 (2020).
- [82] D. Alfe, G. D. Price, and M. J. Gillan, *Phys. Rev. B* **65**, 165118 (2002).
- [83] D. Alfe, *Phys. Rev. B* **79**, 060101(R) (2009).
- [84] J. Bouchet, S. Mazevert, G. Morard, F. Guyot, and R. Musella, *Phys. Rev. B* **87**, 094102 (2013).
- [85] T. Sun, J. P. Brodholt, Y. Li, and L. Vocadlo, *Phys. Rev. B* **98**, 224301 (2018).
- [86] E. Sola and D. Alfe, *Phys. Rev. Lett.* **103**, 078501 (2009).
- [87] Z. Zhang, G. Csanyi, and D. Alfe, *Geochim. Cosmochim. Acta* **291**, 5 (2020).
- [88] L. Burakovsky, D. L. Preston, and R. R. Silbar, *Phys. Rev. B* **61**, 15011 (2000).
- [89] L. Gomez, A. Dobry, Ch. Geuting, H. T. Diep, and L. Burakovsky, *Phys. Rev. Lett.* **90**, 095701 (2003).
- [90] C. Cazorla, M. J. Gillan, S. Taioli, and D. Alfe, *J. Chem. Phys.* **126**, 194502 (2007).
- [91] Z. L. Liu, L. C. Cai, X. R. Chen, and F. Q. Jing, *Phys. Rev. B* **77**, 024103 (2008).
- [92] N. Q. Hoc, T. D. Cuong, B. D. Tinh, and L. H. Viet, *Mod. Phys. Lett. B* **33**, 1950300 (2019).
- [93] F. A. Lindemann, *Phys. Z.* **11**, 609 (1910).
- [94] J. J. Gilvarry, *Phys. Rev.* **102**, 308 (1956).
- [95] S. A. Cho, *J. Phys. F: Met. Phys.* **12**, 1069 (1982).
- [96] S. Zhen and G. J. Davies, *Phys. Status Solidi A* **78**, 595 (1983).
- [97] V. Van Hung, D. T. Hai, and H. K. Hieu, *Vacuum* **114**, 119 (2015).
- [98] N. Q. Hoc, B. D. Tinh, and N. D. Hien, *Mater. Res. Bull.* **128**, 110874 (2020).
- [99] V. V. Hung, N. T. Hoa, and J. Lee, *ASEAN J. Sci. Technol. Dev.* **23**, 27 (2006).
- [100] F. Simon and G. Glatzel, *Z. Anorg. Allg. Chem.* **178**, 309 (1929).
- [101] L. Zeng, S. B. Jacobsen, D. D. Sasselov, M. I. Petaev, A. Vanderburg, M. Lopez-Morales, J. Perez-Mercader, T. R. Mattsson, G. Li, M. Z. Heising, A. S. Bonomo, M. Damasso, T. A. Berger, H. Cao, A. Levi, and R. D. Wordsworth, *Proc. Natl. Acad. Sci. USA* **116**, 9723 (2019).
- [102] H. S. Zapolsky and E. E. Salpeter, *Astrophys. J.* **158**, 809 (1969).
- [103] S. Seager, M. Kuchner, C. A. Hier-Majumder, and B. Militzer, *Astrophys. J.* **669**, 1279 (2007).
- [104] J. J. Fortney, M. S. Marley, and J. W. Barnes, *Astrophys. J.* **659**, 1661 (2007).
- [105] D. Valencia, M. Ikoma, T. Guillot, and N. Nettelmann, *Astron. Astrophys.* **516**, A20 (2010).
- [106] F. W. Wagner, F. Sohl, H. Hussmann, M. Grott, and H. Rauer, *Icarus* **214**, 366 (2011).
- [107] N. Madhusudhan, K. K. M. Lee, and O. Mousis, *Astrophys. J. Lett.* **759**, L40 (2012).
- [108] D. C. Swift, J. H. Eggert, D. G. Hicks, S. Hamel, K. Caspersen, E. Schwegler, G. W. Collins, N. Nettelmann, and G. J. Ackland, *Astrophys. J.* **744**, 59 (2012).
- [109] L. Zeng and D. Sasselov, *Publ. Astron. Soc. Pac.* **125**, 227 (2013).

- [110] A. R. Howe, A. Burrows, and W. Verne, *Astrophys. J.* **787**, 173 (2014).
- [111] C. Dorn, A. Khan, K. Heng, J. A. D. Connolly, Y. Alibert, W. Benz, and P. Tackley, *Astron. Astrophys.* **577**, A83 (2015).
- [112] L. Noack, D. Honing, A. Rivoldini, C. Heistracher, N. Zimov, B. Journaux, H. Lammer, T. V. Hoolst, and J. H. Bredehoft, *Icarus* **277**, 215 (2016).
- [113] A. Mocquet, O. Grasset, and C. Sotin, *Philos. Trans. R. Soc. A* **372**, 20130164 (2014).
- [114] R. L. Akeson, X. Chen, D. Ciardi, M. Crane, J. Good, M. Harbut, E. Jackson, S. R. Kane, A. C. Laity, S. Leifer, M. Lynn, D. L. McElroy, M. Papin, P. Plavchan, S. V. Ramirez, R. Rey, K. von Braun, M. Wittman, M. Abajian, B. Ali *et al.*, *Publ. Astron. Soc. Pac.* **125**, 989 (2013).
- [115] B. A. Buffett, *Geophys. Res. Lett.* **29**, 1566 (2002).
- [116] Q. Li, J. W. Xian, Y. Zhang, T. Sun, and L. Vocadlo, *J. Geophys. Res. Planets* **127**, e2021JE007015 (2022).
- [117] A. M. Dziewonski and D. L. Anderson, *Phys. Earth Planet. Inter.* **25**, 297 (1981).
- [118] G. Masters and D. Gubbins, *Phys. Earth Planet. Inter.* **140**, 159 (2003).
- [119] Y. Zhang, M. Hou, P. Driscoll, N. P. Salke, J. Liu, E. Greenberg, V. B. Prakapenka, and J. F. Lin, *Earth Planet. Sci. Lett.* **553**, 116614 (2021).
- [120] M. Pozzo, C. J. Davies, and D. Alfe, *Earth Planet. Sci. Lett.* **584**, 117466 (2022).
- [121] R. K. Bono, J. A. Tarduno, F. Nimmo, and R. D. Cottrell, *Nat. Geoscience* **12**, 143 (2019).
- [122] T. V. Hoolst, L. Noack, and A. Rivoldini, *Adv. Phys. X* **4**, 1630316 (2019).
- [123] D. Valencia, R. J. O'Connell, and D. Sasselov, *Icarus* **181**, 545 (2006).
- [124] C. Sotin, O. Grasset, and A. Mocquet, *Icarus* **191**, 337 (2007).
- [125] E. Gaidos, C. P. Conrad, M. Manga, and J. Hernlund, *Astrophys. J.* **718**, 596 (2010).
- [126] A. Boujibar, P. Driscoll, and Y. Fei, *J. Geophys. Res. Planets* **125**, e2019JE006124 (2020).
- [127] L. Stixrude, *Philos. Trans. R. Soc. A* **372**, 20130076 (2014).
- [128] Y. Fei, C. T. Seagle, J. P. Townsend, C. A. McCoy, A. Boujibar, P. Driscoll, L. Shulenburger, and M. D. Furnish, *Nat. Commun.* **12**, 876 (2021).
- [129] B. J. Foley and P. E. Driscoll, *Geochem. Geophys. Geosyst.* **17**, 1885 (2016).
- [130] Y. Zhang and J. F. Lin, *Science* **375**, 146 (2022).
- [131] A. Dewaele, P. Loubeyre, F. Occelli, O. Marie, and M. Mezouar, *Nat. Commun.* **9**, 2913 (2018).
- [132] D. E. Fratanduono, R. F. Smith, S. J. Ali, D. G. Braun, A. Fernandez-Pañella, S. Zhang, R. G. Kraus, F. Coppari, J. M. McNaney, M. C. Marshall, L. E. Kirch, D. C. Swift, M. Millot, J. K. Wicks, and J. H. Eggert, *Phys. Rev. Lett.* **124**, 015701 (2020).
- [133] P. F. Weck, P. E. Kalita, T. Ao, S. D. Crockett, S. Root, and K. R. Cochrane, *Phys. Rev. B* **102**, 184109 (2020).
- [134] D. Errandonea, *J. Appl. Phys.* **108**, 033517 (2010).
- [135] D. Errandonea, S. G. MacLeod, L. Burakovsky, D. Santamaria-Perez, J. E. Proctor, H. Cynn, and M. Mezouar, *Phys. Rev. B* **100**, 094111 (2019).
- [136] R. Boehler and M. Ross, *Earth Planet. Sci. Lett.* **153**, 223 (1997).
- [137] A. Hänström and P. Lazor, *J. Alloys Compd.* **305**, 209 (2000).
- [138] J. W. Shaner, J. M. Brown, and R. G. McQueen, *High Pressure in Science and Technology*, edited by C. Homan, R. K. MacCrone, and E. Whalley, (North Holland, Amsterdam, 1984), p. 137.
- [139] L. Vočadlo and D. Alfe, *Phys. Rev. B* **65**, 214105 (2002).
- [140] J. Bouchet, F. Bottin, G. Jomard, and G. Zerah, *Phys. Rev. B* **80**, 094102 (2009).
- [141] Z. L. Liu, X. L. Zhang, and L. C. Cai, *J. Chem. Phys.* **143**, 114101 (2015).
- [142] Q. J. Hong and A. van de Walle, *Phys. Rev. B* **100**, 140102(R) (2019).
- [143] S. Japel, B. Schwager, R. Boehler, and M. Ross, *Phys. Rev. Lett.* **95**, 167801 (2005).
- [144] D. Errandonea, *Phys. Rev. B* **87**, 054108 (2013).
- [145] D. Hayes, R. S. Hixson, and R. G. McQueen, *AIP Conf. Proc.* **505**, 483 (2000).
- [146] L. Vočadlo, D. Alfe, G. D. Price, and M. J. Gillan, *J. Chem. Phys.* **120**, 2872 (2004).
- [147] Q. An, S. N. Luo, L. B. Han, L. Zheng, and O. Tschauner, *J. Phys.: Condens. Matter* **20**, 095220 (2008).
- [148] S. R. Baty, L. Burakovsky, and D. Errandonea, *Crystals* **11**, 537 (2021).
- [149] Y. Zhang, Y. Tan, H. Y. Geng, N. P. Salke, Z. Gao, J. Li, T. Sekine, Q. Wang, E. Greenberg, V. B. Prakapenka, and J. F. Lin, *Phys. Rev. B* **102**, 214104 (2020).
- [150] S. Plimpton, *J. Comput. Phys.* **117**, 1 (1995).
- [151] A. B. Belonoshko, *Geochim. Cosmochim. Acta* **58**, 4039 (1994).
- [152] R. Ahuja, A. B. Belonoshko, and B. Johansson, *Phys. Rev. E* **57**, 1673 (1998).
- [153] A. B. Belonoshko, R. Ahuja, and B. Johansson, *Phys. Rev. Lett.* **84**, 3638 (2000).
- [154] A. B. Belonoshko, R. Ahuja, O. Eriksson, and B. Johansson, *Phys. Rev. B* **61**, 3838 (2000).
- [155] L. Kočí, R. Ahuja, and A. B. Belonoshko, *Phys. Rev. B* **75**, 214108 (2007).
- [156] D. Alfe, M. J. Gillan, and G. D. Price, *J. Chem. Phys.* **116**, 6170 (2002).
- [157] K. Momma and F. Izumi, *J. Appl. Crystallogr.* **44**, 1272 (2011).